Influence of particle disorder and smoothing length on SPH operator accuracy

Geoffroy Chaussonnet, Samuel Braun, Lars Wieth, Rainer Koch, Hans-Jörg Bauer
Institute of Thermal Turbomachines
Karlsruhe Institute of Technology (KIT)
Karlsruhe, Germany
geoffroy.chaussonnet@kit.edu

***Abstract*—SPH consistency and different expression of SPH operators (gradient and Laplacian) accuracy are numerically investigated with regards to particle disorder and smoothing length on different particle distributions (2D and 3D Cartesian and 2D triangular). It is observed that particle disorder deteriorates SPH consistency and adds to the operators a diverging dependency on the smoothing length. Numerical tests evaluate the accuracy of the different operators on perturbed lattices, allowing to establish a rank in terms of robustness against particle disorder.**

I. Introduction

SPH is known to loose consistency on perturbed lattices. Monaghan *et al.* [1] originally showed that the continuous SPH interpolation is second-order consistent, then Quinlan *et al.* [2] highlighted that applying SPH on perturbed lattices will induce an additional *discretization error* (of magnitude $o(h)$ or even divergent in $1/h$, h being the smoothing length) that can be predominant, depending on the level of disorder and the ratio $\Delta x/h$, Δx being the particle spacing.

To circumvent this problem, methods were derived to restore kernel consistency on perturbed lattices such as the Shepard correction, the Mixed Kernel Gradient (MKG) [3] or the RKPM methods [4]. However, exactly retrieving 0-order consistency nullifies a term (see Eq. (3) in [5]) which has a reordering role in simulation of fluids. To the authors knowledge, no robust solution is available to avoid the formation of holes in the lattice when nullifying the stabilizing term and, therefore, the use of correctors is limited to a small range of applications.

Alternatively, it is possible to estimate the error introduced by uncorrected SPH operators in case of particle disorder, and choose the most robust one. Souto-Iglesias *et al.* [6] highlighted the loss of accuracy of gradient and Laplacian operators on a perturbed lattice in Moving Particle Semi-implicit (MPS) method (related to SPH), and Antuono *et al.* [7] defined a measure of particle disorder and estimated its influence on the accuracy of one type of gradient expression.

The present work numerically studies the combined influence of particle disorder and smoothing length on SPH consistency and SPH operators (gradient and Laplacian) accuracy. Next, the paper describes the numerical setup, in particular, the canonical particle disorder. The consistency tests are conducted in the third part and the accuracy of gradient and Laplacian operator are investigated in the fourth and fifth part.

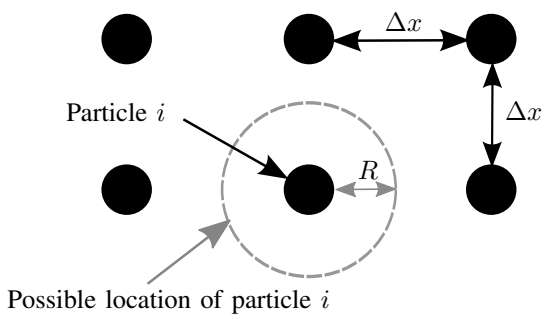

Fig. 1. Schematics of canonical particle disorder

II. Numerical test setup

A. Canonical particle disorder

A canonical particle disorder is defined in 2D (resp. in 3D) as a random shift of particles from their equilibrium state onto a circle (resp. a sphere) of radius $R = \eta\,\Delta x$, for $\eta \in [0, 0.5[$, where Δx is the unperturbed particle interspacing (Fig. 1). The parameter θ is randomly drawn with an equiprobable distribution between 0 and 2π and in 3D an additional random parameter φ is drawn between 0 and π. The distribution of the normalized distance $d/\Delta x$ between two particles is depicted in Fig. 2 for 2D case. If η is sufficiently low, $d/\Delta x$ depends on η only. Its minimum, maximum, mean and standard deviation are 1-2η, 1+2η, 1 and $\approx \eta$ respectively.

B. SPH schemes and notations

In the present paper, subscripts a and b stand for the particle of interest and its neighbors respectively, and their distance is $\boldsymbol{r_{ab}} = \boldsymbol{r}_b - \boldsymbol{r}_a$. The summation symbol always refers to a summation over particles b belonging to the Sphere of Influence (SoI), and the quintic kernel $W(\boldsymbol{r}_{ab}, h)$ is abbreviated to W_{ab}.

Since the method developed at ITS aims to simulate multiphase flows of high density ratio ($\approx$ 1000), the use of traditional SPH operators based on a *density* approach

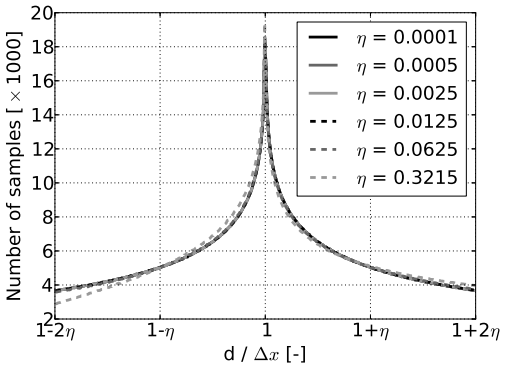

Fig. 2. Density function of normalized distance $d/\Delta x$ in 2D with the canonical disorder.

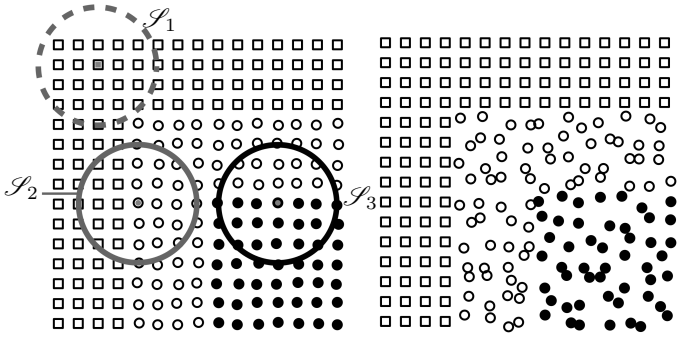

Fig. 3. Top left quarter of the test lattice for 2D case for η = 0.0625 (*left*) and η = 0.3125 (*right*). Symbols □, ○ and ● stand for wall, outer and inner particles respectively

would induce a strong diffusion near the interface over a thickness of the smoothing length. In order to circumvent this effect, operators are expressed with a *volume* approach that corresponds to the original SPH interpolation: $\phi(\boldsymbol{x}) = \int \phi(\boldsymbol{x'})\, W(\boldsymbol{x'} - \boldsymbol{x}, h)\, \mathrm{d}\boldsymbol{x'}$ where ϕ is a scalar field and $\mathrm{d}\boldsymbol{x'}$ an infinitesimal volume. Therefore volume and density are expressed as:

$$V_a = 1/\sum W_{ab} \quad (1)$$

$$\rho_a = m_a \sum W_{ab} \quad (2)$$

where m_a stands for the particle mass. Equations (1) and (2) ensure that the variation of volume and density are just function of neighbors spacing and not of neighbors mass. The SPH method presented in this article is composed of two loops over particle interactions: first, volume and density are calculated using Eqs. (1) and (2) and second, acceleration terms are calculated with the particle volume V_a computed at the first step.

Solid boundaries are taken into account through layers of stationary *wall particles* that avoid to truncate the support volume of wall-adjacent fluid particles. Volume and density of *wall particles* are also computed by Eq. (1) and (2)

C. Test grids

Tests are conducted in 2D (resp. 3D) with particle distribution forming a square (resp. cubic) domain of side length L. The domain is composed of three types of particles as depicted in Fig. 3: (i) unperturbed wall particles with incomplete SoI ($\mathscr{S}_1$), forming a layer of $4h$, (ii) outer perturbed particles with complete SoI ($\mathscr{S}_2$) but influenced by wall particles, over a layer of $4h$ and (iii) inner perturbed particles with complete SoI made only of fluid particles. Numerical tests are conducted on inner particles only, to avoid any deviation due to the influence of wall particles on outer particles. Particle disorder is studied by setting the parameter η to: 10^{-4}, $5{\cdot}10^{-4}$, $2.5{\cdot}10^{-3}$, $1.25{\cdot}10^{-2}$, $6.25{\cdot}10^{-2}$ and 0.3215, as illustrated in Fig. 3.

Two types of lattice are investigated: (i) a cartesian lattice that forms squares in 2D and cubes in 3D, and (ii) a triangular lattice generating equilateral triangles in 2D. The triangular lattice in 3D was not tested due to a tremendously large number of neighbors (≈350) that is prohibitive in engineering applications. The average number of neighbors is 29, 37 and 123 for 2D Cartesian, 2D triangular and 3D Cartesian, respectively.

As the ratio $h/\Delta x$ is kept equal to 1.05, the smoothing length influence is studied by varying the particle interspacing Δx. For consistency tests, the number of particles is kept constant whereas, in the operator tests, L is kept constant, so that the number of particle increases when Δx decreases. The latter method therefore checks the consistency of SPH operators $\mathscr{O}_{SPH}$ in the sense of estimating the residual Ψ:

$$\left| \lim_{\Delta x \to 0} \mathscr{O}_{SPH}(\Delta x) - \mathscr{O}_{ANALYTICAL} \right| = \Psi \quad (3)$$

Finally, the tests are conducted using several grids with the same geometric parameters, in order to keep the total number of data points $N_{grid} \times N_{inner}$ constant and thus preserve the statistical quality.

III. Evaluation of consistencies

A. Definition

Consistency is detailed here as the capacity of the method to recover the j-th derivative of a i-th order polynomial and it is labeled C_i^j. Please note that retrieving a polynomial does not guarantee that its derivative is also recovered. Therefore it is mandatory to check the consistency of polynomial derivative. The first four consistency condition are C_0^0, C_0^1, C_1^0 and C_1^1, and their SPH expression are written as:

$$\sum V_b\, W_{ab} = 1 \quad (4)$$

$$\sum V_b\, \nabla W_{ab} = \mathbf{0} \quad (5)$$

$$\sum V_b\, \boldsymbol{r_{ab}} W_{ab} = \mathbf{0} \quad (6)$$

$$\sum V_b\, \boldsymbol{r_b} \otimes \nabla W_{ab} = \mathbb{I} \quad (7)$$

where ∇, $\otimes$ and $\mathbb{I}$ are the gradient operator, the tensor product and the identity matrix respectively. Fulfilling Eqs. (4) to (7) ensure that at best, SPH can exactly reproduce a linear function and its first derivative.

B. Error functions

Each consistency condition C_i^j is quantified by a local error function ε_i^j at particle a, defined by a L2 norm of the consistency deviation from ideal case:

$$\varepsilon_{0,a}^0 = \left(\sum V_b\, W_{ab} - 1\right)^2 \quad (8)$$

$$\varepsilon_{0,a}^1 = \left|\left|\sum V_b\, \nabla W_{ab} - \mathbf{0}\right|\right|^2 \times h^2 \quad (9)$$

$$\varepsilon_{1,a}^0 = \left|\left|\sum V_b\, \boldsymbol{r_{ab}}\, W_{ab} - \mathbf{0}\right|\right|^2 \times \frac{1}{h^2} \quad (10)$$

$$\varepsilon_{1,a}^1 = \left|\left|\sum V_b\, \boldsymbol{r_b} \otimes \nabla W_{ab} - \mathbb{I}\right|\right|^2 \quad (11)$$

where $\|\boldsymbol{x}\|^2$ and $\|\mathbb{X}\|^2$ represent respectively the magnitude of vector $\boldsymbol{x}$ and an Hilbert-Schmidt operator of the matrix $\mathbb{X}$ of size $n \times n$:

$$\|\mathbb{X}\|^2 = \sum_{(i,j)\in[0,n]^2} |x_{i,j}|^2 \quad (12)$$

Functions ε_i^j are then equal to zero when consistency is perfectly fulfilled, and increases when lacking consistency. Equations (9) and (10) were multiplied or divided by h^2 to recover a non-dimensional error. The overall errors E_i^j are the square root of averaged error functions over inner particles and grid:

$$E_i^j = \sqrt{\langle \varepsilon_i^j \rangle_{N_{\text{grid}} \times N_{\text{inner}}}} \quad (13)$$

C. Results

1) Scaling with h: When particles are regularly spaced (η = 0), all E_i^j are equal to 10^{-20} for all numerical setups, ensuring that the four consistencies are retrieved. Figure 4 displays E_i^j versus h for the maximum disorder η = 0.3215, and shows significant errors independent of h. As E_0^1 and E_1^0 follow the same trend as the one of E_0^0, they are not displayed for the sake of clarity.

Since E_0^0 and E_1^1 are not normalized by h, reducing h does not allow to fulfill C_0^0 and C_1^1, and the error remains constant. E_1^0 is divided by h so that C_1^0 is recovered for $h \to 0$. The worse behavior is attributed to E_0^1 that shows a multiplication by h, leading to a consistency error scaling as $1/h$ and thus diverging for $h \to 0$, as pointed out by Quinlan *et al.* [2]. Finally E_1^1 is larger than the other errors, suggesting that C_1^1 is more sensitive to particle disorder.

2) Scaling with η: Evolution of E_0^0 and E_1^1 versus η is presented in Fig. 5 with h = 1 µm and present a trend which is proportional to η. Errors E_0^0 (so as E_0^1 and E_1^0) are the same in 2D for cartesian and triangular lattice and slightly smaller for the 3D cartesian case, probably due to a larger number of neighbors. E_1^1 is again larger than the other and confirms that C_1^1 is more difficult to obtain.

D. Conclusion of consistency estimation

The four first consistency conditions are always retrieved on regular lattices whereas none of them is perfectly fulfilled on perturbed lattices, and their deviation shows a linear dependence on the canonical disorder η, the largest being C_1^1. When decreasing h to zero, C_1^0 is recovered while C_0^0 and C_1^1 show a constant deviation and C_0^1 diverges. This last point is a serious limitation of SPH when simulating small configurations and performing convergence tests.

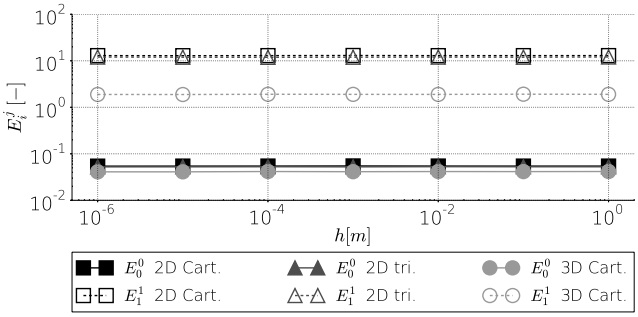

Fig. 4. Consistency errors versus h with η = 0.3215

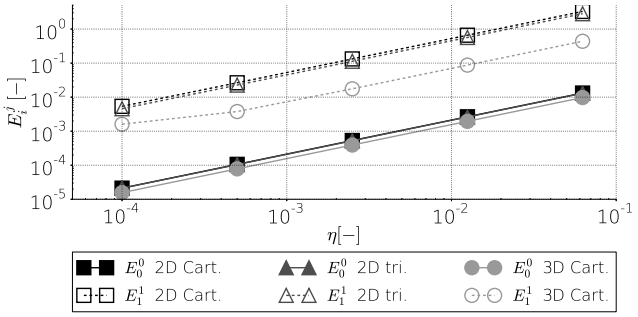

Fig. 5. Consistency errors versus η with h = 1 µm.

IV. Evaluation of gradients

The evaluation of accurate representation of the gradient is conducted by keeping the domain size constant and by decreasing the smoothing length h, corresponding to increasing the number of discretization points. As the behavior of a realistic experiment does not depends on any mesh size, the normalization scale used in this part is the size L of the domain and not h.

A. Types of gradient

Three gradients G_0, G_+ and G_- are evaluated in this work, following a *volume* approach:

$$G_0 : \phi_a \mapsto \nabla_0 \phi_a = \sum V_b\, \phi_b\, \nabla W_{ab} \quad (14)$$

$$G_+ : \phi_a \mapsto \nabla_+ \phi_a = \sum V_b\, (\phi_b + \phi_a)\, \nabla W_{ab} \quad (15)$$

$$G_- : \phi_a \mapsto \nabla_- \phi_a = \sum V_b\, (\phi_b - \phi_a)\, \nabla W_{ab} \quad (16)$$

G_0 correspond to the canonical expression of the gradient in SPH and is directly derived by an integration by parts of the fundamental SPH equation (Eq. 4). The purpose of G_+ is to conserve linear momentum locally by ensuring $\boldsymbol{f}_{ab} = -\boldsymbol{f}_{ba}$ where $\boldsymbol{f}_{ab}$ is the elementary force that particle b exerts on particle a. For instance, in the case of the pressure force,

$\boldsymbol{f}_{ab}^{(p)} = V_a\, V_b (p_b + p_a) \nabla W_{ab}$ and $\boldsymbol{f}_{ab}^{(p)} = -\boldsymbol{f}_{ba}^{(p)}$. G_- is constructed to ensure that the gradient of a constant function is zero, even if C_0^1 is not verified. Note that G_- and G_0 do not locally conserve linear momentum.

B. Role of C_0^1 in gradient estimation

Writing the gradient operators (G_K) in a general form $\nabla_K \phi_a = \sum V_b \left(\phi_b + K\, \phi_a\right) \nabla W_{ab}$ leads to:

$$\nabla_K \phi_a = \sum V_b\, \phi_b\, \nabla W_{ab} + K\, \phi_a \sum V_b\, \nabla W_{ab} \tag{17}$$

The first term of the RHS of Eq. 17 is the canonical gradient and the second term shows the C_0^1 condition. It suggests that when C_0^1 is not fulfilled, the three gradients are not identical and the deviation from G_0 is proportional to ϕ_a for $\nabla_+ \phi_a$ and $\nabla_- \phi_a$. In addition, when considering a constant field F_0, the gradients $\nabla_0 F_0$ and $\nabla_+ F_0$ are explicitly:

$$\nabla_0 F_0 = F_0 \sum V_b\, \nabla W_{ab} \tag{18}$$

$$\nabla_+ F_0 = 2\, F_0 \sum V_b\, \nabla W_{ab} \tag{19}$$

which shows that (i) G_0 and G_+ cannot predict a zero gradient for a constant field when C_0^1 is not fulfilled and (ii) G_+ is two times more sensitive to the C_0^1 condition than G_0 due to the factor 2 in Eq. (19).

C. Types of fields

The three studied scalar fields are constant (F_0), linear (F_1) and quadratic (F_2) with the following expressions:

$$F_0(x) = K_x \tag{20}$$

$$F_1(x) = K_x\, \xi \tag{21}$$

$$F_2(x) = K_x\, \xi^2/2 \tag{22}$$

so that K_x is the value, the normalized slopes and normalized curvatures for F_0, F_1 and F_2, respectively, and $\xi = x/L$ the normalized x coordinate. To study the gradient intensity K_x was varied over the following values: 0.01, 0.1, 1, 10 and 100.

D. Error functions

The deviation between SPH gradients and analytical ones is measured through the local non-dimensional error:

$$\lambda_{x_j}^i (G_K) = \frac{1}{N_i^2} \left(\nabla_{K,x_j} F_i - \frac{\partial F_i}{\partial x_j} \right)^2 \tag{23}$$

where ∇_{K,x_j} stands for the x_j component of G_K. The term N_i is a normalization factor equal to K_x/L for the constant field F_0 and to the magnitude of the analytical gradient for the two other fields. Note that all $\partial F_i/\partial x_j$ are zero, except:

$$\frac{\partial F_1}{\partial x} = \frac{K_x}{L}, \quad \text{and} \quad \frac{\partial F_2}{\partial x} = \frac{K_x\, x}{L^2} \tag{24}$$

Like for the consistency study, the global error $\Lambda_{x_j}^i (G_K)$ is determined by summing over inner particles and grids (Eq. 13).

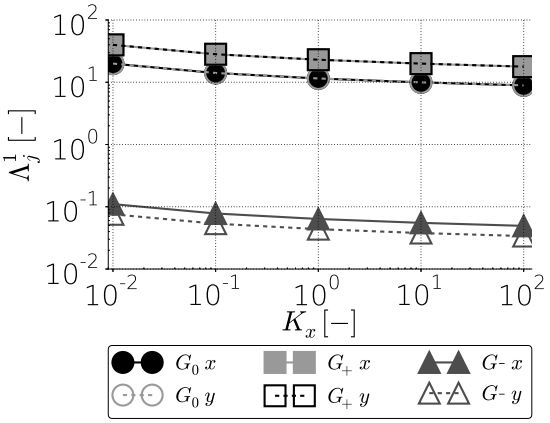

Fig. 7. Comparison of Λ_x^1 and Λ_y^1 on a 2D cartesian lattice

E. Results

1) Influence of lattice: As illustrated in Fig. 6, all investigated lattices (2D cartesian, 2D triangular and 3D cartesian) have the same trends. 2D cases have very similar errors and 3D cases show generally errors ≈15% lower than 2D cases. This is possibly due to a larger number of neighbors that reduces the smoothing length error. Based on these observations, the next figures will display results of 2D Cartesian lattices only.

2) Directivity: Although the investigated gradients are only oriented towards x ($\partial F_i/\partial y = \partial F_i/\partial z = 0$), it is observed that K_x influences Λ_y^i and Λ_z^i, so that deviation is the same in the three dimensions, as illustrated in Fig. 7. This effect is due to the isotropic essence of the kernel that homogeneously redistributes the error into other dimensions. This observation implies that the direction of the gradient is influenced by particle disorder, and could not distinguishes different order of magnitudes along different axis, (*e.g.* the gradient of the function $f(x, y) = 1000\, x + y$ could not exhibit a dependence on y due to the noise on the x component).

3) Constant field: Figure 8 displays Λ_x^0 versus h, η and K_x. When η = 0, all operators show no deviation (Fig. 8(b)). For $\eta \neq 0$, error is proportional to $1/h$, and proportional to η. Surprisingly, Λ_x^0 slightly decreases when K_x increases (Fig. 8(c)) whereas Eqs. (18) and (19) predict no dependence on K_x (= F_0) as the error is normalized by K_x. This may be explained by the fact that lower K_x are more sensible to floating point truncation error. As expected, the deviation of G_+ is twice larger than the one of G_0, and since G_- exactly predicts the zero gradient, it is not plotted.

The error is expressed as a function of h, η and K_x under the form $\Lambda_x^0(h, \eta, K_x) = a_1\, h^{a_2}\, \eta^{a_3}\, K_x^{a_4}$ and (a_1, a_2, a_3, a_4) is fitted over all cases, leading to:

$$\Lambda_x^0(G_0) = 3.12\ 10^{-3}\ h^{-1.03}\ \eta^{0.985}\ K_x^{-0.0857} \tag{25}$$

$$\Lambda_x^0(G_+) = 6.11\ 10^{-3}\ h^{-1.04}\ \eta^{0.987}\ K_x^{-0.0848} \tag{26}$$

Equations (25) and (26) indicate an acceptable proportionality to the term η/h and a weak dependence on K_x, and confirm

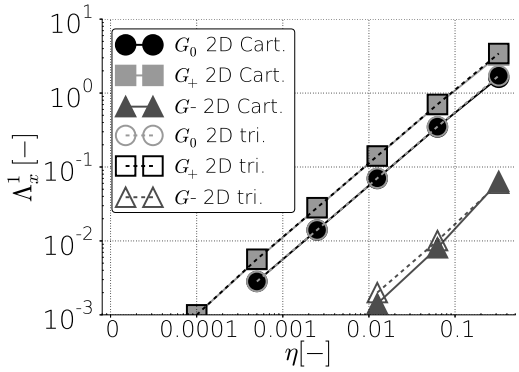

(a) 2D Cartesian/Triangular comparison of Λ_x^1 versus η with h = 0.001 m

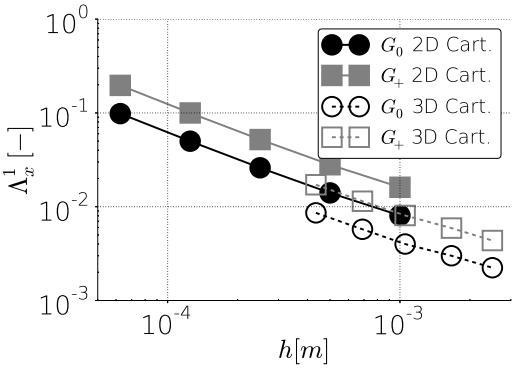

(b) Cartesian 2D/3D comparison of Λ_x^1 versus h with η = 0.0025

Fig. 6. Influence of lattice type on SPH gradient (K_x = 1)

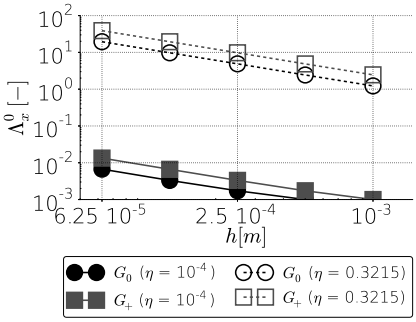

(a) Λ_x^0 versus h (K_x = 1)

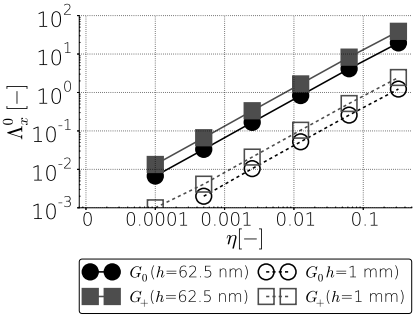

(b) Λ_x^0 versus η (K_x = 1)

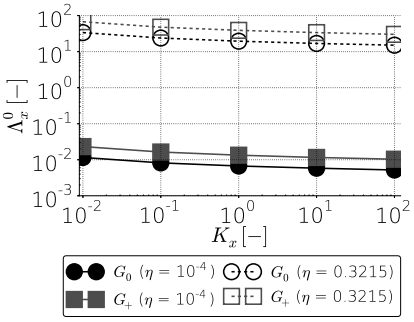

(c) Λ_x^0 versus K_x (h = 6.25 10^{-5} m)

Fig. 8. Influence of smoothing length and particle disorder on SPH gradients of a constant field, on a 2D cartesian lattice

the factor 2 between G_+ and G_0.

4) Linear field: The residual Λ_x^1 is plotted in Fig. 9 versus h, η and K_x. Fitting the errors with h, η and K_x leads to:

$$\Lambda_x^1(G_0) = 4.36\ 10^{-3}\ h^{-0.941}\ \eta^{0.988}\ K_x^{-0.0847} \quad (27)$$

$$\Lambda_x^1(G_+) = 9.12\ 10^{-3}\ h^{-0.936}\ \eta^{0.989}\ K_x^{-0.0854} \quad (28)$$

$$\Lambda_x^1(G_-) = 1.70\ 10^{-1}\ h^{-0.0406}\ \eta^{1.15}\ K_x^{-0.0903} \quad (29)$$

Figure 9 and Eqs. (27) to (29) show the same trends as with the constant field: the error is approximately proportional to η/h for G_0 and G_+. Surprisingly, G_- behaves much better that the two other as it presents (i) no influence of h and (ii) non-zero deviations only for large particle disorder or strong gradients.

5) Quadratic field: Errors Λ_x^2 are displayed in Fig. 10. The same trends as for a linear field with slightly lower error values are found. As for the case of constant field, G_+ errors are two times larger than G_0: $\Lambda_x^2(G_+) \approx 2 \cdot \Lambda_x^2(G_0)$.

F. Conclusion of gradient estimation

The operator G_+ shows the largest error which is twice as large as the one of G_0. This is probably due to sign "+" in Eq. (15) that sums errors on ϕ_a and ϕ_b. The operator G_- shows the lowest relative deviation and a low dependence on the smoothing length h. From a numerical point of view, it is the best to use. However it does not locally conserve linear momentum, and a more detailed study is necessary to estimate if this drawback overwhelms the benefits retrieved from its superiority regarding particle disorder.

V. Evaluation of Laplacians

A. Types of Laplacian

1) MCG: The Laplacian proposed by [8] and [9] is referred to as MCG and is given by:

$$\Delta_{MCG}(\boldsymbol{u})_a = \frac{2}{\pi}(d+2)\sum V_b \frac{\boldsymbol{r}_{ab}\cdot\boldsymbol{v}_{ab}}{r_{ab}^2+\theta^2}\nabla W_{ab} \quad (30)$$

where d and $\theta = 0.01\,h^2$ are the dimension and a term to avoid a zero denominator, respectively. The term $\boldsymbol{r}_{ab}\cdot\boldsymbol{v}_{ab}$ is the scalar product between particle positions $\boldsymbol{r}_{ab} = \boldsymbol{r}_b - \boldsymbol{r}_a$ and particle velocities $\boldsymbol{v}_{ab} = \boldsymbol{v}_b - \boldsymbol{v}_a$. The prefactor $1/\pi$ was not in the original formulation but is added in the present work to match the analytical Laplacian. As $\Delta_{MCG}(\boldsymbol{u_a})$ is oriented along the inter-particle axis, its stress force is axial

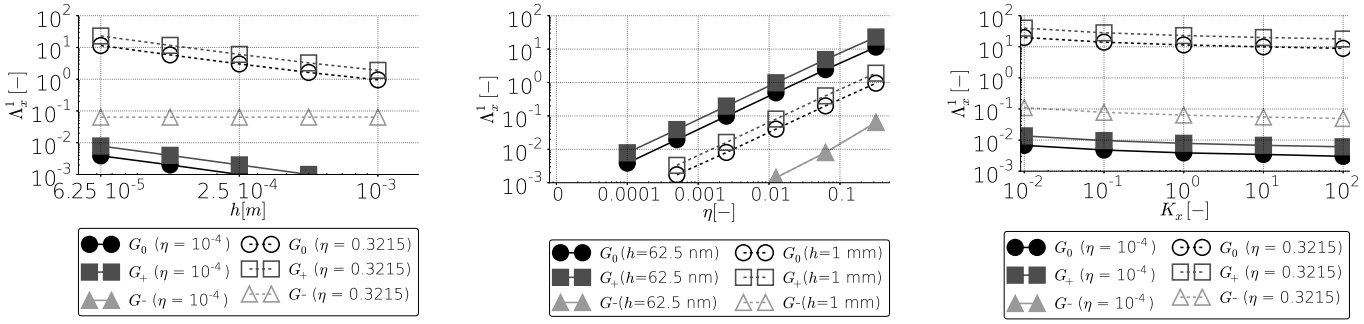

(a) Λ_x^1 versus h (K_x = 1) (b) Λ_x^1 versus η (K_x = 1) (c) Λ_x^1 versus K_x (h = 6.25 10^{-5} m)

Fig. 9. Influence of smoothing length and particle disorder on SPH gradients of a linear field, on a 2D cartesian lattice

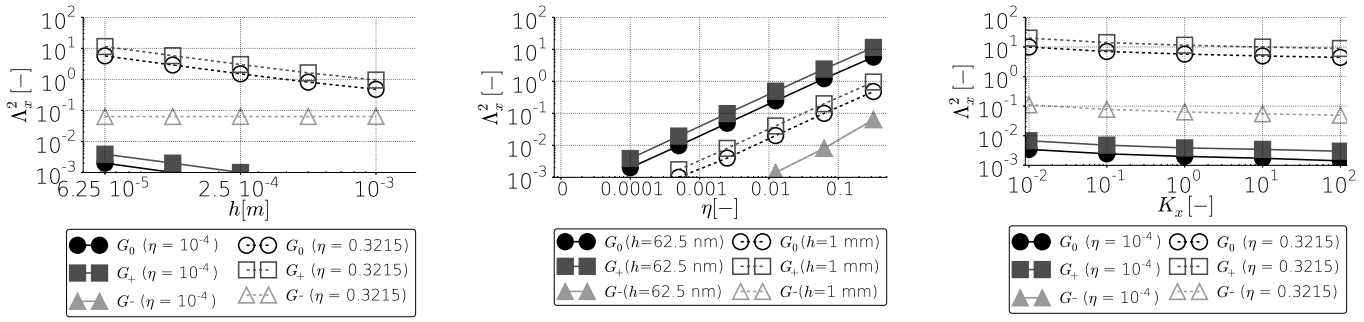

(a) Λ_x^2 versus h (K_x = 1) (b) Λ_x^2 versus η (K_x = 1) (c) Λ_x^2 versus K_x (h = 6.25 10^{-5} m)

Fig. 10. Influence of smoothing length and particle disorder on SPH gradients of a quadratic field, on a 2D cartesian lattice

and the local angular momentum is conserved.

2) MEA: This Laplacian estimation, labeled MEA, was proposed by [10] and [11]:

$$\Delta_{MEA}(\boldsymbol{u})_a = 2\sum V_b \frac{\nabla W_{ab}\cdot \boldsymbol{r}_{ab}}{r_{ab}^2+\eta^2}\boldsymbol{v}_{ab} \tag{31}$$

It is oriented along the velocity difference $\boldsymbol{v}_{ab}$ so that angular momentum is not locally conserved.

B. Type of fields

As the most important role of the Laplacian is to model viscous stress based on the second derivative of the velocity, it is applied here to a vector field. Investigated fields are the same as for gradients investigation (Eqs. 20 to 22) but applied to the x component of the velocity:

$$\boldsymbol{U_0}(x) = (K_x, 0, 0) \tag{32}$$
$$\boldsymbol{U_1}(x) = (K_x\,\xi, 0, 0) \tag{33}$$
$$\boldsymbol{U_2}(x) = (K_x\,\xi^2/2, 0, 0) \tag{34}$$

The Laplacian thus corresponds to a second derivative with respect to x.

C. Error function

The general error function is defined as:

$$\omega_{x_j}^i(\Delta_{\mathscr{L}}) = \frac{1}{N^2}\left(\Delta_{\mathscr{L},x_j}\boldsymbol{U_i} - \sum_k \frac{\partial^2 U_{i,x_j}}{\partial x_k^2}\right)^2 \tag{35}$$

where $\Delta_{\mathscr{L},x_j}$ is the x_j component of the Laplacian $\mathscr{L}$ (MCG or MEA). The analytical Laplacian (right term in parenthesis) is equal to $\partial^2 U_{i,x}/\partial x^2$ when $x_j = x_k = x$ and is zero otherwise, and the normalization factor N is equal to K_x/L^2. The global error Ω is calculated according to Eq. (13).

D. Results

1) Type of lattice: Trends are the same on 2D Cartesian and 2D triangular lattices with linear fields. With quadratic fields, MCG shows a higher deviation on triangular lattices compared to Cartesian ones (Fig. 11(a)). The same finding are valid for the comparison of 2D/3D Cartesian configurations, although 3D lattices show approximately an error 20% lower than 2D ones, as shown in Fig. 11(b).

2) Directivity: A comparison between Ω_x^2 and Ω_y^2 versus K_x is displayed in Fig. 12. It shows that for MCG, both direction have same trends with the same order of magnitude, whereas the MEA operator shows zero deviation on its y component: $\Omega_y^{1,2}(\Delta_{MEA}) = 0$. This can be explained by the

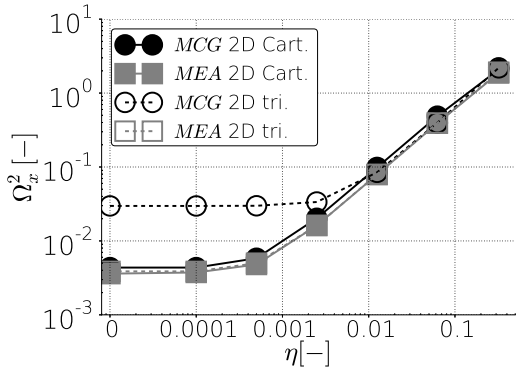

(a) Cartesian/Triangular 2D comparison of Ω_x^2 versus η with h = 0.001 m

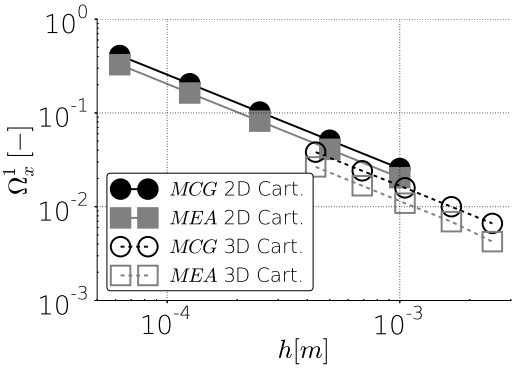

(b) Cartesian 2D/3D comparison of Ω_x^1 versus h with η = 0.0025

Fig. 11. Influence of lattice type (K_x = 1) on Laplacian estimation

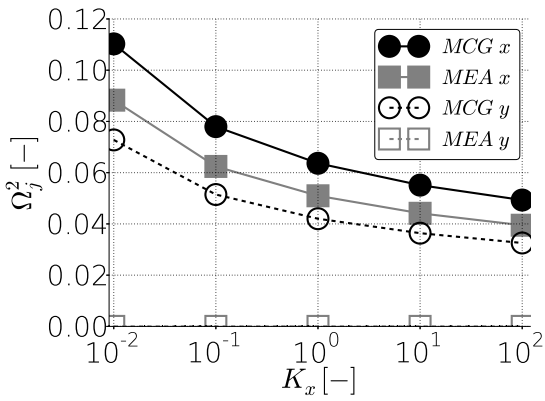

Fig. 12. Comparison of Ω_x^2 and Ω_y^2 on a 2D cartesian lattice

fact that Δ_{MEA} is oriented along $\boldsymbol{v}_{ab}$ (Eq. 31) so that a zero component for the velocity induces a zero component for the Laplacian. This characteristic of the MEA operator thus ensures that the inaccuracy due to particle disorder is kept along $\boldsymbol{v}_{ab}$ and is not diffused in other dimensions, leading to a better resolution of the operator directivity.

3) Constant field: Due to the presence of the term $\boldsymbol{v}_{ab}$ in both expressions, the SPH Laplacian of a constant field is always zero, independently of the smoothing length, particle disorder or the field absolute value.

4) Linear field: As depicted in Fig. 13, both Laplacian operators follow the same trends as gradients operators for each investigated parameters: they are proportional to η/h and slightly decrease with K_x. Fitting Ω_x^1 with the expression $\Omega_x^1(h,\eta,K_x) = a_1\, h^{a_2}\, \eta^{a_3}\, K_x^{a_4}$ leads to:

$$\Omega_x^1(\Delta_{MCG}) = 8.89\ 10^{-3}\ h^{-1.01}\ \eta^{0.979}\ K_x^{-0.0844} \quad (36)$$

$$\Omega_x^1(\Delta_{MEA}) = 6.07\ 10^{-3}\ h^{-1.03}\ \eta^{0.986}\ K_x^{-0.0849} \quad (37)$$

which confirms the proportionality to η/h and low influence of K_x. In addition, it shows an error for the MEA operator to be 18% lower than for MCG, which is visible in Figs. 13 for any of the investigated parameters. Finally, no disorder induces an exact prediction of the Laplacian for both operators.

5) Quadratic field: Figures 14 display Ω_x^2 versus h, η and K_x and show that MEA and MCG have the same trends. Proportionality to $1/h$ is lost for a strong disorder, and linearity with η is lost for low disorder. In particular, both operators are not exact on regular lattices (Fig. 14(b)). Regarding K_x, a slight decrease is observed when K_x increases. Finally, MEA behaves slightly better with an global error 17% lower than MCG.

E. Conclusion of Laplacian estimation

Both operator present the same trends with regards to investigated parameters and, contrary to gradients, there is no clear advantages for MCG or MEA. On 2D Cartesian lattices with linear and quadratic fields, MEA shows an error $\approx$ 20% lower than MCG for all investigated parameters. On 2D Triangular lattices (no curves shown here) and linear fields, MEA and MCG deliver the same error, whereas MCG gives higher errors on low to moderate particle disorder ($0 \leqslant \eta < 10^{-2}$) with quadratic fields.

VI. Conclusion

SPH consistency was studied versus the particle disorder η, the smoothing length h, with a constant $h/\Delta x$ ratio. On a a regular lattice, the four first consistency conditions (C_0^0, C_0^1, C_1^0 and C_1^1) are fulfilled and independent of h. On the contrary, perturbed lattices bring more complexity: the deviation of consistency conditions (i) increases with particle disorder and (ii) depends on the smoothing length with different behavior depending on the consistency condition. It is indeed observed that C_0^0 and C_1^1 are independent of h while C_1^0 is proportional to h and C_0^1 diverges with $1/h$, which may be critical

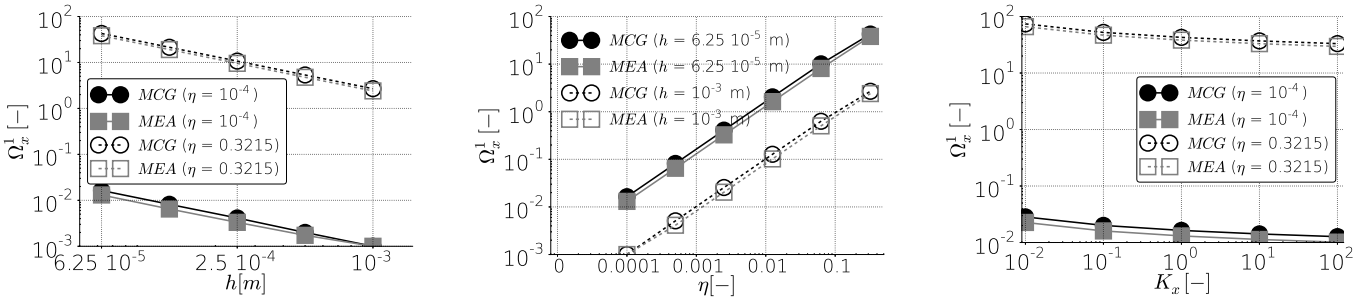

(a) Ω_x^1 versus h (K_x = 1) (b) Ω_x^1 versus η (K_x = 1) (c) Ω_x^1 versus K_x (h = 6.25 10^{-5} m)

Fig. 13. Influence of smoothing length and particle disorder on SPH Laplacians of a linear field, on a 2D cartesian lattice

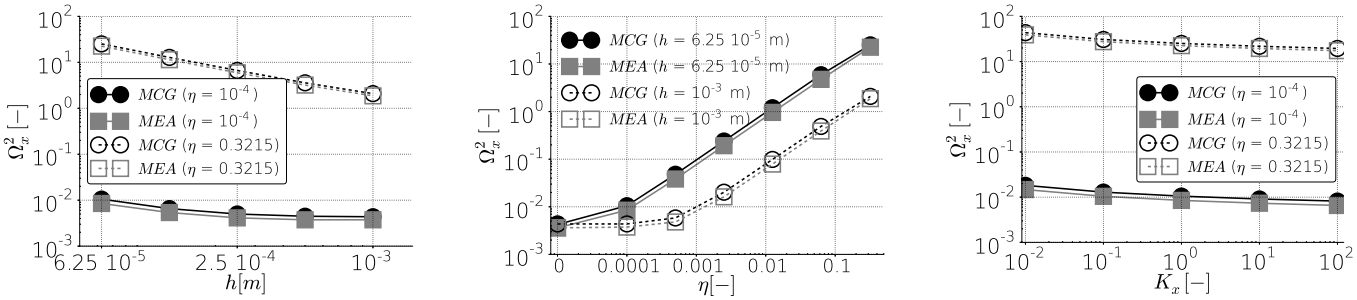

(a) Ω_x^2 versus h (K_x = 1) (b) Ω_x^2 versus η (K_x = 1) (c) Ω_x^2 versus K_x (h = 6.25 10^{-5} m)

Fig. 14. Influence of smoothing length and particle disorder on SPH Laplacians of a quadratic field, on a 2D cartesian lattice

when simulating small configurations. The importance of C_0^1 condition for gradients calculation was also highlighted.

SPH operators accuracy (gradient and Laplacian) were also studied versus η, h and the non-dimensional parameter K_x corresponding to a field magnitude, slope or curvature. The operator G_- showed the best behavior with (i) an error of two orders of magnitude lower than G_0 and G_+, and (ii) a low dependency on h. Regarding the Laplacian, both operators, MEA and MCG show the same trends with a little advantage for MEA whose error function is generally 30% lower than MCG one. These considerations are purely numerical and should be completed by a physical study: given that G_- and MEA do not locally conserve the linear and angular momentum respectively, it must be confirmed that their numerical advantages are still significant with regards to physical considerations.

Finally, different particle distributions were investigated (2D and 3D Cartesian and 2D triangular) and the same trends were observed.

REFERENCES

[1] J.J. Monaghan. Smoothed particle hydrodynamics. *Annual Review of Astronomy and Astrophysics*, 30:543 – 574, 1992.

[2] N. J. Quinlan, M. Basa, and M. Lastiwka. Truncation error in mesh-free particle methods. *International Journal for Numerical Methods in Engineering*, 66(13):2064–2085, 2006.

[3] J. Bonet and T.-S. L. Lok. Variational and momentum preservation aspects of smooth particle hydrodynamic formulations. *Computer methods in applied mechanics and engineering*, 180:97 – 115, 1999.

[4] W. K. Liu, S. Jun, and Y. F. Zhang. Reproducing kernel particle methods. *International journal for numerical methods in fluids*, 20(8-9):1081–1106, 1995.

[5] S. Marrone, A. Colagrossi, M. Antuono, G. Colicchio, and G. Graziani. An accurate sph modeling of viscous flows around bodies at low and moderate reynolds numbers. *Journal of Computational Physics*, 245:456–475, 2013.

[6] A. Souto-Iglesias, F. Macià, L. M. González, and J. L. Cercos-Pita. On the consistency of mps. *Computer Physics Communications*, 184(3):732–745, 2013.

[7] M. Antuono, B. Bouscasse, A. Colagrossi, and S. Marrone. A measure of spatial disorder in particle methods. *Computer Physics Communications*, 185(10):2609–2621, 2014.

[8] R.A. Gingold and J.J. Monaghan. Smoothed particle hydrodynamics: theory and application to non-spherical stars. *Monthly Notices of the Royal Astronomical Society*, 181:375 – 389, 1977.

[9] P.W. Cleary and J.J. Monaghan. Conduction modelling using smoothed particle hydrodynamics. *Journal of Computational Physics*, 148:227 – 264, 1999.

[10] J.P. Morris, P.J. Fox, and Y. Zhu. Modeling low reynolds number incompressible flows using sph. *Journal of Computational Physics*, 136:214 – 226, 1997.

[11] P. Español and M. Revenga. Smoothed dissipative particle dynamics. *Phys. Rev. E*, 67:026705, Feb 2003.